DOI: 10.1021/ma9017857

Macromolecules
ARTICLE

Correlation of Structure Changes in the Water-Induced Phase Transitions of Poly(ethylenimine) Viewed from Molecular, Crystal, and Higher-Order Levels As Studied by Simultaneous WAXD/SAXS/Raman Measurements

Tomoko Hashida,[†] Kohji Tashiro,*[,†] Kazuki Ito,[‡] Masaki Takata,[‡,§] Sono Sasaki,[§] and Hiroyasu Masunaga[§]

[†]*Department of Future Industry-oriented Basic Science and Materials, Toyota Technological Institute, Tempaku, Nagoya 468-8511, Japan,* [‡]*RIKEN SPring-8 Center, Kouto, Sayo, Hyogo 679-5148, Japan, and* [§]*Japan Synchrotron Radiation Research Institute, Kouto, Sayo, Hyogo 679-5198, Japan*

Received August 9, 2009; Revised Manuscript Received October 26, 2009

ABSTRACT: Simultaneous measurements of WAXD, SAXS, and Raman spectra have been performed during the water-induced phase transitions of poly(ethylenimine) (PEI). As is well-known, PEI transforms among four kinds of crystalline forms by absorbing water: anhydrate (EI/water = 1/0), hemihydrate (1/0.5), sesquihydrate (1/1.5), and dihydrate (1/2). The chain conformation changes from double helix in the anhydrate (0) to planar-zigzag form in the hemi- (0.5), sesqui- (1.5), and dihydrates (2). The structuctural changes in the crystalline region during the water-induced phase transitions have been found to induce also the remarkable changes in the higher-order structure of stacked lamellae on the basis of the detailed comparison between WAXD and SAXS data. The anhydrate (0) composed of double helices showed the long period of 81 Å. When the anhydrate (0) started to transfer to the hemihydrate (0.5), the two types of long periods, 75 and 159 Å, were observed. The 159 Å period appeared only temporarily in the transition process from anhydrate (0) to hemihydrate (0.5). In the transition from hemihydrate (0.5) to sesquihydrate (1.5) and to dihydrate (2) the long period changed to 64 Å (0.5 and 1.5) and 61 Å (2). These SAXS profile changes have been reproduced quantitatively on the basis of a stacked lamellar structural model with paracrystalline disorder taken into consideration.

Introduction

Poly(ethylenimine) [PEI, $-(CH_2CH_2NH)_n-$] exhibits water-induced phase transitions among four crystalline hydrates: anhydrate (molar ratio EI/water = 1/0), hemihydrate (1/0.5), sesquihydrate (1/1.5), and dihydrate (1/2), as shown in Figure 1.[1−3] The chain conformation of the anhydrate (0) is a double helix formed by N−H···N hydrogen bonds between the neighboring PEI chains. By absorbing water, the double helix changes to a pair of single chains of planar-zigzag conformation with the N−H···O and O−H···N hydrogen bonds formed among water molecules and PEI chains.[1−3] Depending on the water content included in the crystal lattice, the packing structures of PEI and water molecules are different among the hemi- (0.5), sesqui- (1.5), and dihydrates (2). In this way the double helix of PEI is stabilized by intermolecular hydrogen bonds, and it transforms to the parallel packing of single chains through the rearrangements of hydrogen bonds between polymer and water molecules. Such a transition between double helices and single chains is quite unique among many synthetic polymers.

In a series of papers,[4−8] we have investigated the structural changes of PEI in the hydration and heating processes by measuring the vibrational spectra and wide-angle X-ray diffraction (WAXD) patterns. On the basis of these experimental data, the changes in molecular conformation and crystal lattice during the phase transitions were clarified in a concrete manner. The relative strengths of hydrogen bonds in the hydrates were estimated by analyzing the infrared and Raman bands characteristic of each hydrate. In addition to these crystalline phase transitions, the water-induced crystallization was also revealed to occur in the amorphous region during the transitions.[6] It might be expected, therefore, the PEI sample should become fully crystalline at the end of hydration process. Actually, however, it is difficult to get such a fully crystallized sample because of the disturbance by the entanglements of polymer chains in the amorphous phase, though the degree of crystallinity becomes remarkably high in the hydrated state.[6] By performing the temperature-dependent measurement of infrared spectra under various water contents, the effect of temperature and water content on the phase transitional behavior was also studied extensively.[7] Using these experimental results, we built up a phase diagram of the PEI/water system as functions of water content and temperature.[7] On the basis of this phase diagram, it is possible to predict the transitional behaviors in both the hydration and heating processes. In fact, the predicted phase transitions were confirmed quite reasonably by performing the X-ray diffraction measurements under the various temperature/humidity conditions.[8]

In this way we have been studying the changes in the crystal lattice of the PEI−water system in detail. How about the relation between the crystal and high-order structure? It might be reasonable to speculate that the higher-order structure is also affected more or less by the phase transitions in the crystalline region, as known from many examples describing the intimate relationship between the structural changes in crystal lattice and higher-order structure.[9−17] In these cases the thermally activated molecular chains in the crystal lattice experience the translational motion as well as the rotational (librational) motion coupled with the conformational change through the torsional motion around the skeletal CC bonds. These motions do not affect only the

*To whom correspondence should be addressed.

 Published on Web 12/08/2009

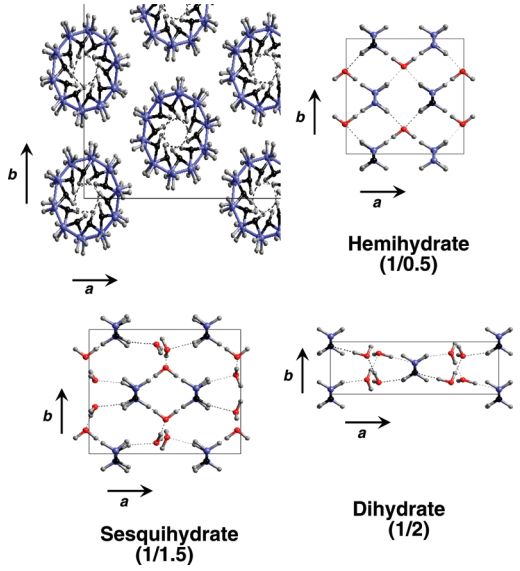

Figure 1. Crystal structures of poly(ethylenimine).

crystal lattice but also the whole shape and stacking morphology of the crystalline lamellae and then the physical property of the bulk samples. In the case of PEI, too, the study of the hierarchical relationship between the molecular conformation, crystal lattice, and higher-order structure is important for controlling the physical property, although the structural transitions occur *via* water absorption mechanism, different from the above-mentioned many other cases.

As described in the present paper, we have performed the simultaneous measurement of small-angle X-ray scattering (SAXS), wide-angle X-ray diffraction (WAXD), and Raman spectra in the hydration process to clarify the hierarchical relationship. Since the transition occurs rapidly during the water supply, high-speed measurement is required for the WAXD, SAXS, and Raman spectra. The WAXD and SAXS measurements were performed using the high-flux synchrotron X-ray beam as well as the X-ray instrument in the laboratory. The Raman spectra were obtained at the same time with the X-ray measurements for getting the information on molecular structural changes. The SAXS patterns were analyzed on the basis of the stacked lamellar structural model with paracrystalline disorder taken into account. It may be said that the present study will make a significant contribution to the development of the structural study of solid-state PEI in the humid atmosphere.

Experimental Section

Linear PEI was obtained by the acid hydrolysis of poly(*N*-acetylethylenimine) [M_w: 500 000 g/mol] which was supplied by Dow Chemical Co. Ltd.[18] Uniaxially oriented films were prepared by stretching the melt-quenched sample in the dry ice/methanol bath. The samples were kept *in vacuo* for 7 days at 35 °C to obtain the anhydrate (0) sample.

The simultaneous time-resolved measurements of WAXD, SAXS, and Raman spectra were performed in the hydration process of PEI at the beamline BL45XU of SPring-8, Hyogo, Japan, where a high-flux synchrotron X-ray beam of 0.90 Å wavelength was generated by an undulator. Figure 2a shows a schematic illustration of the measurement system. The sample of ca. 150 μm thickness was set into the cell with a pair of thin Mylar films (2 μm thickness). Water was supplied quickly to the bottom of this cell, and the WAXD/SAXS/Raman measurements were started immediately. The SAXS, WAXD, and Raman data were collected for 1 s at every 10 s interval. In this experiment the sample was exposed continuously in the water vapor atmosphere,

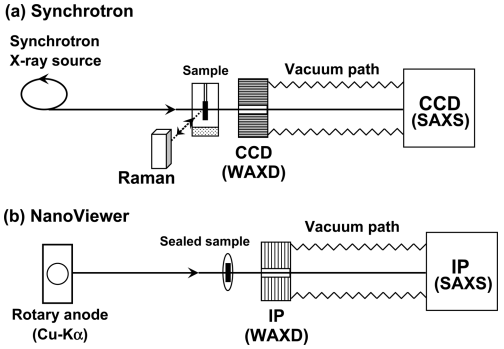

Figure 2. Schematic illustrations of the measurement systems: (a) simultaneous WAXD/SAXS/Raman measurement using synchrotron system; (b) simultaneous measurement of WAXD and SAXS using NanoViewer in the laboratory.

and the transition proceeded up to the sesquihydrate (1.5). Since the sample was relatively thick, it was not possible to reach the fully hydrated dihydrate (2) during the experimental time. The 2-dimensional WAXD pattern was detected using an arrayed fiber-optic taper coupled CCD detector (arrayed FOT-CCD detector),[19,20] which was set at a distance of 126 mm from the sample cell. The 2D SAXS pattern was measured using an X-ray image intensifier with CCD installed at a distance of 2541 mm from the sample position. For the Raman spectral measurement, a laser beam of 633 nm wavelength was incident to the sample using an optical fiber, and the backscattered Raman signals were collected with the same optical fiber, where the Raman spectrometer of Lambda Vision Co. Ltd., Japan, was used.

The synchrotron experiment gave the SAXS and WAXD data of high intensity. But, as will be seen later, the SAXS data were not very clear due to too strong central scatterings (probably coming from some voids included in the sample). Then the simultaneous measurements of WAXD and SAXS were also performed using Nanoviewer (RIGAKU) in the laboratory. The measurement system is shown in Figure 2b. The finely focused X-ray beam of Cu Kα line (λ = 1.54 Å) was incident to the sample. Imaging plates were used as the detectors for WAXD and SAXS data. The sample-to-detector distances were 30 mm for WAXD and 560 mm for SAXS. Since the X-ray exposure time was long, the hydration was assumed to have been enough well equilibrated at each humidity condition to give some particular hydrate phases. The sample was sealed off perfectly immediately after the supply of a certain amount of water. The SAXS pattern changes were essentially the same as those of synchrotron experiments but with clearer images in the central parts.

Results and Discussion

Simultaneous WAXD/SAXS/Raman Measurements Using Synchrotron System. Figure 3 shows the time dependence of WAXD and SAXS patterns in the hydration process of the oriented PEI sample, which were measured using synchrotron system. Since the two panels were set separately in the arrayed FOT-CCD detector, the WAXD patterns given in Figure 3a are combinations of two images taken by these two separate panels. The WAXD pattern at the starting point was that of anhydrate (0). By absorbing water, the X-ray scattering intensities of the anhydrate (0) decreased and the reflections of the hemihydrate (0.5) started to appear. The WAXD pattern at 17 min corresponds to that of hemihydrate (0.5). After that, the reflections of sesquihydrate (1.5) started to appear and coexisted with those of hemihydrate (0.5). The transition from sesquihydrate (1.5) to dihydrate (2) occurred too slowly to trace completely in this experiment.

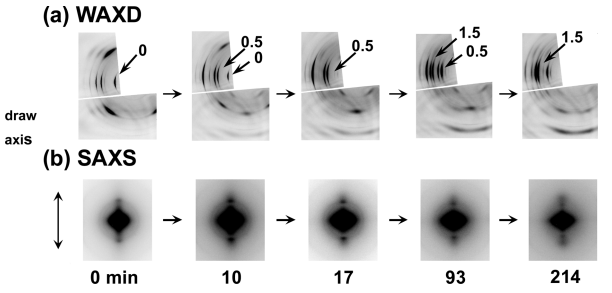

Figure 3. Time dependence of WAXD and SAXS patterns of uniaxially oriented PEI sample in the hydration process measured with the synchrotron system: (a) WAXD and (b) SAXS patterns.

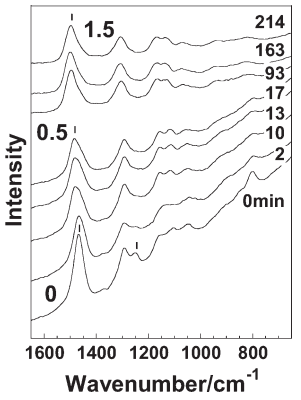

Figure 4. Time-dependent Raman spectral change in the hydration process of PEI measured simultaneously with the WAXD and SAXS data shown in Figure 3.

In the SAXS patterns shown in Figure 3b, the meridional scattering peaks were detected, which changed the positions by hydration. The long period changed from 74 Å of the anhydrate (0), to 83 Å of the hemihydrate (0.5), and to 90 and 66 Å for the mixture of hemi- (0.5) and sesquihydrates (1.5).

Figure 4 shows the time dependence of Raman spectra measured simultaneously with the synchrotron WAXD and SAXS data. The spectrum at 0 min corresponds to that of the anhydrate (0). The bands at 800, 1250, and 1465 cm^{-1}, characteristic of the anhydrate (0), rapidly decreased in intensity by hydration. Since it was difficult to separate the bands of hemi- (0.5) and sesquihydrates (1.5) in the frequency region of 1482−1493 cm^{-1}; these bands were analyzed as a combined band.[5] The Raman band intensities of anhydrate (0), hemi- (0.5), and sesquihydrates (1.5) are plotted against time in a logarithmic scale in comparison with the changes in WAXD and SAXS data, as shown in Figure 5. When the WAXD reflections changed from anhydrate (0) to hemihydrate (0.5) and to sesquihydrate (1.5), the Raman band intensity was found to change in parallel. The SAXS long period of anhydrate (0) was 74 Å at the starting point. It became apparently continuously longer during the transition from anhydrate (0) to hemihydrate (0.5). When the anhydrate (0) disappeared totally at around 10 min, the long period was about 83 Å. Then, the two long periods were observed at 90 and 66 Å during the transition from hemihydrate (0.5) to sesquihydrate (1.5).

In this way, a good correlation was observed between the molecular, crystal, and higher-order structures in the process of water-induced phase transitions. In the SAXS measurement using synchrotron X-ray beam, however, the central part of SAXS patterns was detected too strongly

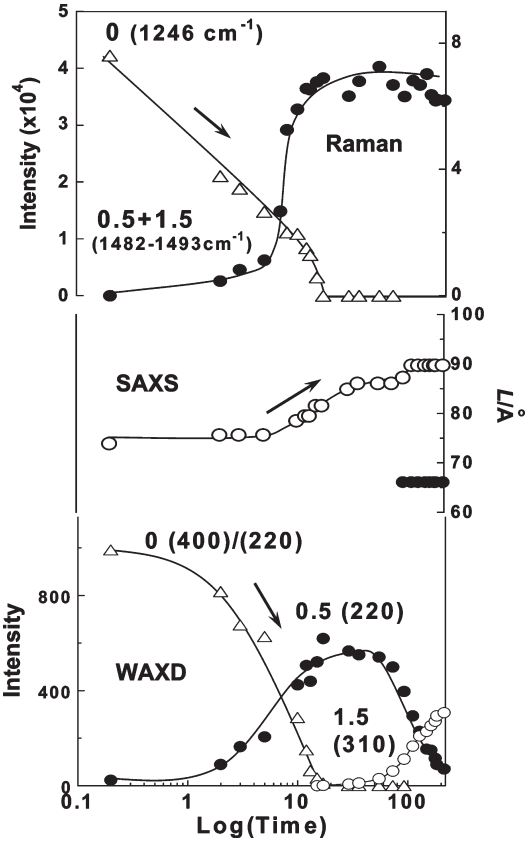

Figure 5. Time dependence of the Raman band intensities, the SAXS long period, and the WAXD intensities of the hydrates in the hydration process of PEI.

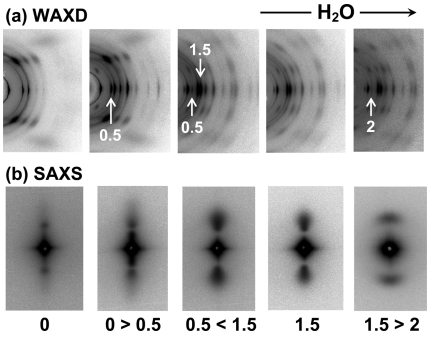

Figure 6. (a) WAXD and (b) SAXS patterns of uniaxially oriented PEI samples with the various hydrates.

even in a quite short exposure time to perform the detailed analysis of the integrated intensity profiles in a quantitative manner. In addition, the transition from sesquihydrate (1.5) to dihydrate (2) was not observed in this measurement. Then we were challenged again by the simultaneous WAXD/SAXS measurements in the laboratory using thicker samples (ca. 500 μm) to increase the signal-to-noise ratio.

Figure 6 shows the WAXD and SAXS patterns thus collected using the Nanoviewer. In this experiment the sample was sealed perfectly immediately after the supply of a certain amount of water, and then the WAXD and SAXS measurement was made with relatively long X-ray exposure time. A series of X-ray scattering patterns given in Figure 6 are those taken for long time at different constant water contents. It may be reasonable to assume that the sample was enough well in the equilibrated state at

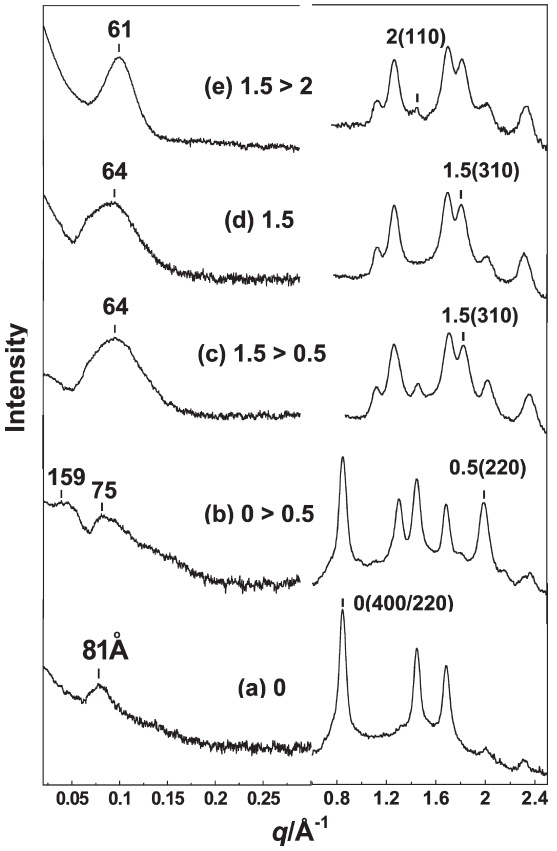

Figure 7. Equatorial WAXD and meridional SAXS profiles measured for uniaxially oriented PEI samples with various hydrates (refer to Figure 6).

each water content. The WAXD profiles along the equatorial line and the SAXS profiles along the meridional line are shown in Figure 7. As seen in the WAXD data of high q range, where $q = (4\pi/\lambda)\sin(\theta)$ for the scattering angle 2θ and X-ray wavelength λ, the transitions between the anhydrate (0), hemihydrate (0.5), sesquihydrate (1.5), and dihydrate (2) were observed cearly in the hydration process. The corresponding SAXS patterns are shown in Figure 6b. The long period observed for the anhydrate (0) was 81 Å. In the transition from the anhydrate (0) to hemihydrate (0 > 0.5), the plural number of scatterings were detected along the meridional line, corresponding to the long periods of 75 and 159 Å. (The long period peak of 159 Å could not be detected in the synchrotron experiment because of too strong central scattering.)

When the anhydrate (0) disappeared completely as known from the WAXD data, the long period peak of 159 Å disappeared at the same time. At the stage of hemi- and sesquihydrates mixture (Figure 7c) or the pure sesquihydrate (Figure 7d), the broad peak of 64 Å long period existed. Then the long period changed to 61 Å when the dihydrate started to appear (1.5 > 2). In the synchrotron experiment, the peak was observed also at 90 Å, which was not detected in Figure 6. While the synchrotron experiment was to trace the structural change *in situ* during the hydration process, the laboratory experiment measured the structure attained at equilibrated states. Therefore, by comparing these two different experimental results, we may say that some special aggregation state might appear on the way of transition by hydration, but the details are not known at present. We need to perform more highly qualified synchrotron experiment again. In the present paper the analysis of higher-order

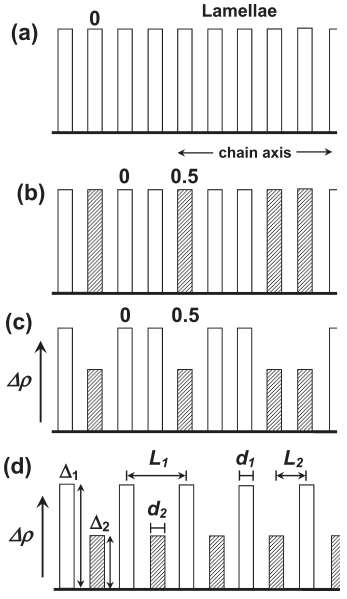

Figure 8. Schematic illustration of the stacked lamellar structure: (a) the anhydrate (0), (b) mixture of anhydrate (0) and hemihydrates (0.5), (c) the model equivalent to (b) but with the electron density distribution taken into account, and (d) the structural model of alternately stacked lamellae with different electron densities.

structure will be made for the SAXS data taken at equilibrated states.

Models of Higher-Order Structures. As pointed out above, the SAXS long period 159 Å was detected only temporarily in the transition from anhydrate (0) to hemihydrate (0.5). This peak disappeared when all the anhydrates (0) transferred to the hydrates (0.5 and 1.5). The long period 159 Å is nearly double of the value 81 Å detected for the anhydrate (0). To interpret this appearance of two types of long periods, we calculated the SAXS intensity profiles based on the stacked lamellar structural model. As shown in Figure 8a, the dry PEI sample is assumed to consist of stacked lamellae of anhydrate (0). By absorbing water, some of lamellae may transfer to the hemihydrate (0.5), as shown in Figure 8b. This may occur statistically randomly. When a double helix in the anhydrate (0) transfers to a couple of planar-zigzag chains in the hemihydrate (0.5), the electron density along the chain axis changes from 25 (0) to 16 (0.5).[1−3] Although the lamellar stacking structure is the same as (b), Figure 8c considers the electron density, where the height corresponds to the electron density difference between the lamellar and amorphous phases. This model given in (c) is complicated and difficult to calculate the corresponding X-ray scattering pattern. But, as already reported,[21,22] this statistically disordered model is essentially equivalent to that shown in Figure 8d or the alternately arranged model of the two kinds of lamellae of different electron densities.

The lamellae are assumed to have the sharp edges. The relative electron density of the original anhydrate lamella is Δ_1, and that of hydrate lamella is Δ_2. The d_1 and d_2 indicate the thicknesses of a main lamella and an inserted one, respectively. The long period L_2 is assumed to be a half of the original period L_1; $L_2 = L_1/2$. If the second kind of disorder is introduced to the model shown in Figure 8d, the scattering intensity $I(q)$ is expressed by eq 1:[23,24]

$$I(q) = P(q)L(q) \quad (1)$$

where $P(q)$ is a particle factor and $L(q)$ is a lattice factor. $P(q)$ is a square of Fourier transform of structure unit $\rho(x)$ shown

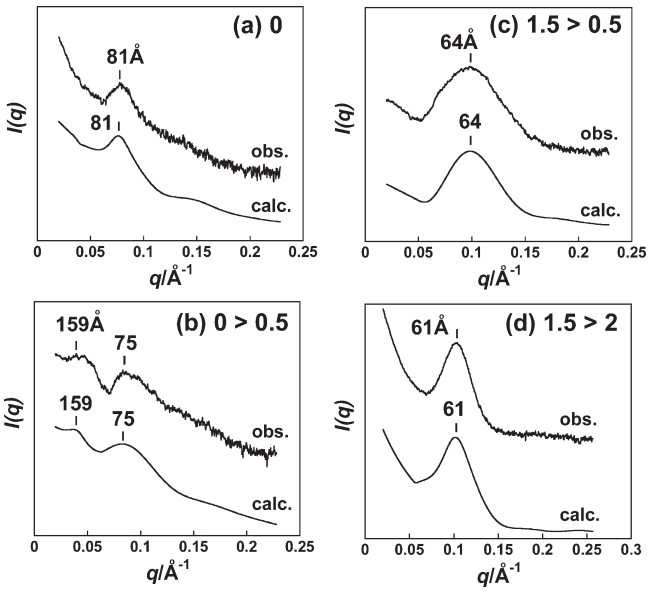

Figure 9. Comparison of the observed SAXS profiles of PEI with the profiles simulated for the stacked lamellar structure model: (a) anhydrate (0), (b) the mixture of anhydrate (0) and hemihydrate (0.5) (0 > 0.5), (c) the mixture of hemi- and sesquihydrates (1.5 > 0.5) and the sesquihydrate (1.5), and (d) the mixture of sesqui- and dihydrates (1.5 > 2).

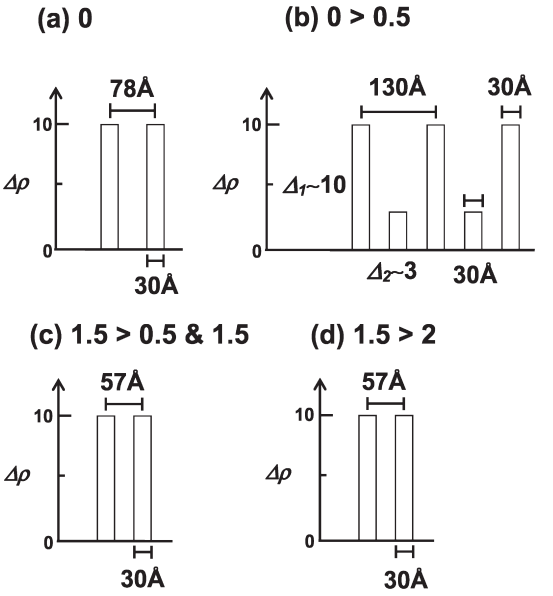

Figure 10. Stacked lamellar models obtained for (a) anhydrate (0), (b) the mixture of anhydrate and hemihydrate (0 > 0.5), (c) the mixture of hemi- and sesquihydrates (1.5 > 0.5) and the sesquihydrate (1.5), and (d) the mixture of sesqui- and dihydrates (1.5 > 2). The electron density $\Delta\rho$ is a relative one.

in eq 2 and is given by eq 3.

$$\rho(x) = \begin{cases} \Delta & (-d/2 \le x \le d/2) \\ 0 & (x < -d/2,\ d/2 < x) \end{cases} \tag{2}$$

$$\begin{aligned} P(q) &= \left| \int_{-\infty}^{\infty} \rho(x) \mathrm{e}^{-iqx}\, \mathrm{d}x \right|^2 \\ &= \left| \frac{2\Delta_1 \sin(d_1 q/2)}{q} + \frac{2\Delta_2 \sin(d_2 q/2)}{q} \exp(-iLq/2) \right|^2 \\ &= 4[{\Delta_1}^2 \sin^2(d_1 q/2) + 2\Delta_1\Delta_2 \cos(Lq/2) \\ &\quad \sin(d_1 q/2) \sin(d_2 q/2) + {\Delta_2}^2 \sin^2(d_2 q/2)]/q^2 \end{aligned} \tag{3}$$

The lattice factor $L(q)$ is a square of Fourier transform of one-dimensional periodicity of lamellae with the second kind of disorder and is given by eq 4.

$$\begin{aligned} L(q) &= \frac{1 - \exp(-4\pi^2 g^2 h^2)}{[1 - \exp(-2\pi^2 g^2 h^2)]^2 + 4 \sin^2(\pi h) \exp(-2\pi^2 g^2 h^2)} \\ &= \frac{\sinh(q^2 {\sigma_L}^2/2)}{\cosh(q^2 {\sigma_L}^2/2) - \cos(Lq)} \end{aligned} \tag{4}$$

where the Gaussian distribution is assumed for the long period L, and g ($= \sigma_L/L$) is a measure of the second kind of disorder and σ_L is the standard deviation. h is given as $h = Lq/2\pi$. Substituting eqs 3 and 4 into eq 1, the scattering intensity $I(q)$ is expressed by eq 5.

$$I(q) = \frac{4[{\Delta_1}^2 \sin^2(d_1 q/2) + 2\Delta_1\Delta_2 \cos(Lq/2) \sin(d_1 q/2) \sin(d_2 q/2) + {\Delta_2}^2 \sin^2(d_2 q/2)] \sinh(q^2 {\sigma_L}^2/2)}{q^2[\cosh(q^2 {\sigma_L}^2/2) - \cos(Lq)]} \tag{5}$$

The parameters Δ_1, Δ_2, etc., were adjusted to reproduce the observed SAXS profiles as reasonably as possible.

The comparison between the observed and calculated SAXS profiles is shown in Figure 9a–d. Figure 10 exhibits the resultant structural models. The anhydrate (0) sample possesses the stacked lamellar structure of the averaged long period 78 Å and the thickness ca. 30 Å. In the case of mixture of anhydrate (0) and hemihydrate (0.5) (Figure 9b), two sorts of lamellae with the electron density ratio 10:3 are existent as shown in Figure 10b, where the long periods are 130 and 65 Å. The thickness of the lamellae is 30 Å. The SAXS profiles of 1.5 > 0.5 and 1.5 give the models shown in Figure 10c,d. The long period is 57 Å, and the lamellar thickness is 30 Å. The electron densities of these hydrates are 16.9 (0.5), 21.2 (1.5), and 23.9 (2). Since the relative electron densities of these hydrates are similar to each other, the lamellae cannot be distinguished each other among these three types of hydrates.

The structural parameters thus obtained are shown in Figure 11. The g factor, a measure of second kind of disorder, increases in the transition process from anhydrate (0) to hemihydrate (0.5) and to sesquihydrate (1.5), indicating the disorder of the lamellar stacking structures in the process of water-induced phase transition. When the dihydrate (2) starts to appear, however, the g factor decreases, meaning that the lamellar stacking structure becomes ordered again in the transition to hydrate (2).

The models shown in Figure 10 take the difference of electron density into consideration. In the actual case the structure of Figure 10 can be expressed more realistically as the statistically disordered lamellar stacking structure as shown in Figure 12. The anhydrate (0) sample has the lamellar stacking structure of the long period 78 Å and the lamellar thickness 30 Å (Figure 12a). Some of the lamellae transform to those of hemihydrate (0.5) by hydration, and the long period changes slightly (Figure 12b). Further

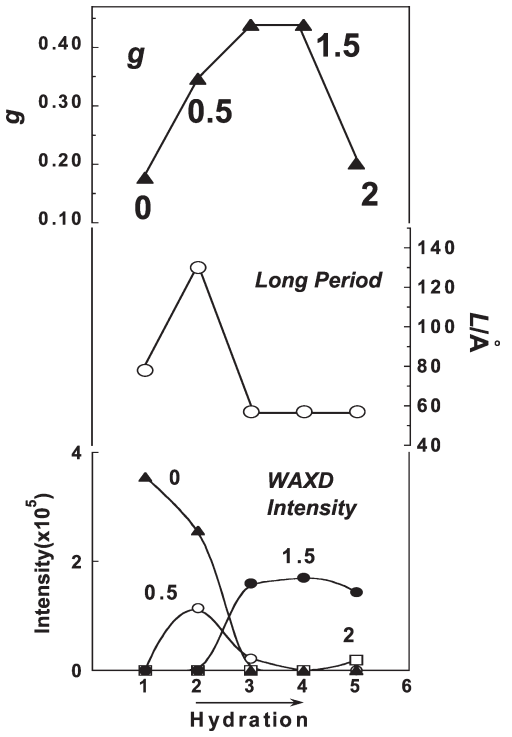

Figure 11. Changes of g factor, long period L, and WAXD peak intensities evaluated for the various hydrate states of PEI (refer to Figure 10).

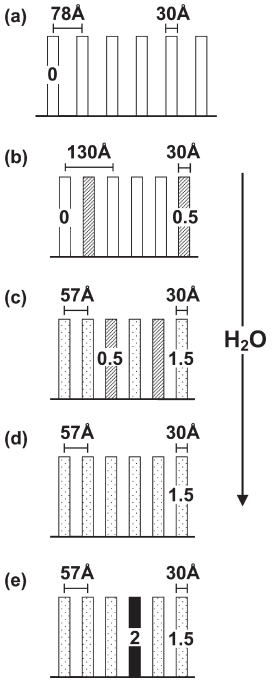

Figure 12. More realistically illustrated higher-order structural models corresponding to the various hydrate states of PEI. These models give essentially the same SAXS profiles calculated for the models shown in Figure 10.

absorption of water induces the transitions from hemihydrate (0.5) to sesquihydrate (1.5) and dihydrate (2), but the lamellar stacking structure is almost preserved: the long period 57 Å and the lamellar thickness 30 Å.

About the Lamellar Thickness and Structural Change. In the phase transition of PEI, the chain conformation changes remarkably between the helical and planar-zigzag forms.

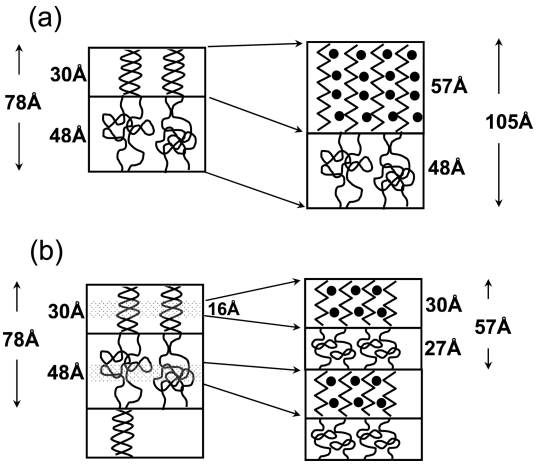

Figure 13. Illustration of the higher-order structural change in the hydration process of PEI from the anhydrate (0) to the mixture of anhydrate (0) and hemihydrates (0.5). (a) The double helical parts are assumed to change totally to the planar-zigzag chains. The lamellar thickness increases by about twice and the long period increases from 78 to 105 Å. This model cannot reproduce the observed SAXS profile (Figures 7 and 9). (b) Central parts of double helices transform to the planar-zigzag chains, and the other parts change to the amorphous phase. At the same time the amorphous phase transforms partially to the crystalline hydrate phase. The long period changes from 78 to 57 Å.

The fiber period of double helix is 4.79 Å as observed in X-ray diffraction pattern, but the actual period of single helical chain component is 9.58 Å consisting of 5 monomeric units.[1−3] In other words, the helical pitch per monomeric unit is 9.58/5 = 1.92 Å. On the other hand, the fiber period of planar-zigzag chain conformation is 7.31 Å and consists of 2 monomeric units along the chain axis. The pitch is 7.31/2 = 3.66 Å/monomer unit. Therefore, when the anhydrate (0) transforms to the hemihydrates (0.5), the lamellar thickness should increase by about twice (3.66/1.92) as long as the chain axis is kept in the transition. In the above-mentioned calculation of lamellar thickness, as shown in Figures 10 and 12, the lamellar thickness of 30 Å is kept unchanged in the transition process. In the structural transition, the whole part of double helix may not change to the regular zigzag chains, but some portions may be disordered to become the amorphous state, resulting in the lamellar thickness of 30 Å. At the same time, it is needed to remember that the amorphous region can be crystallized by hydration.[6] The original amorphous thickness is about 48 Å, since the long period is 78 Å and lamellar thickness is 30 Å. Therefore, it might be possible for the amorphous phase to change partially to the crystalline phase of 30 Å thickness. The long period of the anhydrate (0) is 78 Å, while it is 57 Å in the hydrate phase. By considering all these situations, we may draw the structural change of stacked lamellae in a more concrete way as shown in Figure 13. In this figure, the anhydrate part of lamella changes to the crystalline (hydrate) and amorphous regions. The original amorphous phase changes also to the similar structure. As a result, the alternating structure of 30 Å lamella and 27 Å amorphous region is finally attained.

Conclusion

In the present study, the higher-order structural changes have been investigated in relation with the molecular and crystal structural changes during the water-induced phase transitions of PEI by means of simultaneous WAXD/SAXS/Raman measurements. When the phase transitions occurred from anhydrate (0) to hemihydrate (0.5), sesquihydrate (1.5), and dihydrate (2), the SAXS patterns changed dramatically. The long period of

anhydrate (0) observed was 81 Å. When the anhydrate (0) started to transfer to the hemihydrate (0.5), the two long periods of 75 and 159 Å appearred. In the transition from hemihydrate (0.5) to sesquihydrate (1.5) the long period changed to 64 Å. The dihydrate (2) showed the long period 61 Å. To interpret these phenomena, the SAXS intensity profiles were calculated based on the stacked lamellar structural model with the paracrystalline disorder taken into account.

PEI is characteristic in such a sense that it shows the water-induced crystalline phase transitions between the double helix and planar-zigzag chains. In this transition process, at the same time, the higher-order structure changes remarkably as described in the present paper. For the various crystalline polymers, the stacked lamellar structure is well-known to be affected more or less in the thermally induced phase transitions due to the drastically enhanced thermal motion of molecular chains in the high-temperature region.[9−17] In the present PEI case, the water molecules play a role to induce such a drastic motion of molecular chains to cause the change in lamellar stacking structure as well as the changes in the molecular conformation and the packing structure of these chains. For clarifying the details of location and movement of water molecules in the PEI samples, the usage of such techniques as solid-state NMR and wide- and small-angle neutron scatterings will be helpful, which are now trying to be performed.

Acknowledgment. This work was financially supported by the MEXT "Collaboration with Local Communities" project (2005−2009) and the Sasakawa Scientific Research Grant from the Japan Science Society.

References and Notes

(1) Chatani, Y.; Tadokoro, H.; Saegusa, T.; Ikeda, H. *Macromolecules* **1981**, *14*, 315.
(2) Chatani, Y.; Kobatake, T.; Tadokoro, H.; Tanaka, R. *Macromolecules* **1982**, *15*, 170.
(3) Chatani, Y.; Kobatake, T.; Tadokoro, H. *Macromolecules* **1983**, *16*, 199.
(4) Hashida, T.; Tashiro, K.; Aoshima, S.; Inaki, Y. *Macromolecules* **2002**, *35*, 4330.
(5) Hashida, T.; Tashiro, K. *Polymer* **2007**, *48*, 7614.
(6) Hashida, T.; Tashiro, K.; Inaki, Y. *Polymer* **2003**, *44*, 1721.
(7) Hashida, T.; Tashiro, K.; Inaki, Y. *J. Polym. Sci., Part B: Polym. Phys.* **2003**, *41*, 2937.
(8) Hashida, T.; Tashiro, K. *Macromol. Symp.* **2006**, *242*, 262.
(9) Tashiro, K.; Sasaki, S. *Prog. Polym. Sci.* **2003**, *28*, 451.
(10) Tashiro, K.; Tanaka, R. *Polymer* **2006**, *47*, 5433.
(11) Masunaga, H.; Sasaki, S.; Tashiro, K.; Hanesaka, M.; Tanaka, M.; Inoue, K.; Ohta, N.; Yagi, N. *Polym. J.* **2007**, *39*, 1281.
(12) Tashiro, K.; Sasaki, S.; Saragai, S. *J. Polym. Sci., Part B: Polym. Phys.* **2004**, *42*, 4175.
(13) Tashiro, K. *Chin. J. Polym. Sci.* **2007**, *25*, 73.
(14) Gowd, E.; Bhoje; Shibayama, N.; Tashiro, K. *Macromolecules* **2008**, *41*, 2541.
(15) Yang, X. N.; Tan, S. S.; Li, G.; Zhou, E. *Macromolecules* **2001**, *34*, 5936.
(16) Kawakami, D.; Ran, S. F.; Burger, C.; Avila-Orta, C.; Sics, I.; Hsiao, B. S.; Kikutani, T. *Macromolecules* **2006**, *39*, 2909.
(17) Ran, S. F.; Hsiao, B. S.; Agarwal, P. K.; Verma-Nair, M. *Polymer* **2003**, *44*, 2385.
(18) Tanaka, R.; Ueoka, I.; Takaki, Y.; Kataoka, K.; Saito, S. *Macromolecules* **1983**, *16*, 849.
(19) Ito, K.; Fujisawa, T.; Iwata, T. *AIP Proc.* **2007**, *879*, 1160.
(20) Ito, K.; Fujisawa, T.; Iwata, T. *Nucl. Instrum. Methods* **2007**, *A 582*, 673.
(21) Hama, H.; Tashiro, K. *Polymer* **2003**, *44*, 6973.
(22) Hama, H.; Tashiro, K. *Polymer* **2003**, *44*, 2159.
(23) Hosemann, R.; Bagchi, S. N. *Direct Analysis of Diffraction by Matter*; North-Holland: Amsterdam, 1962.
(24) Reinfold, C.; Fischer, E. W.; Peterlin, A. *J. Appl. Phys.* **1964**, *35*, 71.